



## City Research Online

### City, University of London Institutional Repository

---

**Citation:** Georgantzia, E., Vardanega, P. & Kashani, M. M. (2025). Modelling low-cycle fatigue behaviour of structural aluminium alloys. *Bulletin of Earthquake Engineering*, 23(4), pp. 1737-1758. doi: 10.1007/s10518-025-02097-x

This is the published version of the paper.

This version of the publication may differ from the final published version.

---

**Permanent repository link:** <https://openaccess.city.ac.uk/id/eprint/34471/>

**Link to published version:** <https://doi.org/10.1007/s10518-025-02097-x>

**Copyright:** City Research Online aims to make research outputs of City, University of London available to a wider audience. Copyright and Moral Rights remain with the author(s) and/or copyright holders. URLs from City Research Online may be freely distributed and linked to.

**Reuse:** Copies of full items can be used for personal research or study, educational, or not-for-profit purposes without prior permission or charge. Provided that the authors, title and full bibliographic details are credited, a hyperlink and/or URL is given for the original metadata page and the content is not changed in any way.

---

---





# Modelling low-cycle fatigue behaviour of structural aluminium alloys

Evangelia Georgantzia<sup>1</sup> · Paul J. Vardanega<sup>2</sup> · Mohammad M. Kashani<sup>3</sup>

Received: 21 May 2024 / Accepted: 6 January 2025  
© The Author(s) 2025

## Abstract

Recently, use of 6000 series aluminium alloys in braced frame structures has been increased due to their superior structural properties. Fracturing of braces as a result of low-cycle fatigue has a major impact on nonlinear behaviour of structures under earthquake loading. Therefore, modelling low-cycle fatigue life, i.e., number of reversals to failure, is important to understanding braced-frame structural performance. To date, there are no readily available methods for predicting the low-cycle fatigue behaviour of 6000 series aluminium alloys. This research study aims to provide structural engineers with a computationally efficient approach to assess aluminium alloy structures in the context of potential low cycle fatigue. For this purpose, 18 low-cycle high amplitude fatigue tests (up to  $\pm 6\%$  strain amplitude) were conducted to establish strain–life relationships for 6082-T6, 6063-T6 and 6060-T5 aluminium alloys. The obtained experimental results were then used to calibrate a low-cycle fatigue life model to capture the fracture behaviour of the studied materials. The comparison of experimental results and predicted fatigue behaviour shows the capability of the proposed model to predict to a high degree of precision the onset of fracture and the overall low-cycle fatigue behaviour of material.

**Keywords** Aluminium alloys · Low-cycle fatigue · Cyclic degradation · Fatigue life estimation · Constitutive modelling

---

✉ Evangelia Georgantzia  
evangelia.georgantzia@city.ac.uk

Paul J. Vardanega  
p.j.vardanega@bristol.ac.uk

Mohammad M. Kashani  
mehdi.kashani@soton.ac.uk

<sup>1</sup> Department of Engineering, School of Science & Technology, City St George's, University of London, Tait Building, Northampton Square, London EC1V 0HB, UK

<sup>2</sup> School of Civil, Aerospace and Design Engineering, Faculty of Science and Engineering, University of Bristol, Queen's Building, University Walk, Bristol BS8 1TR, UK

<sup>3</sup> Boldrewood Innovation Campus, School of Engineering, Faculty of Engineering and Physical Sciences, University of Southampton, Building 178, Southampton SO16 7QF, UK

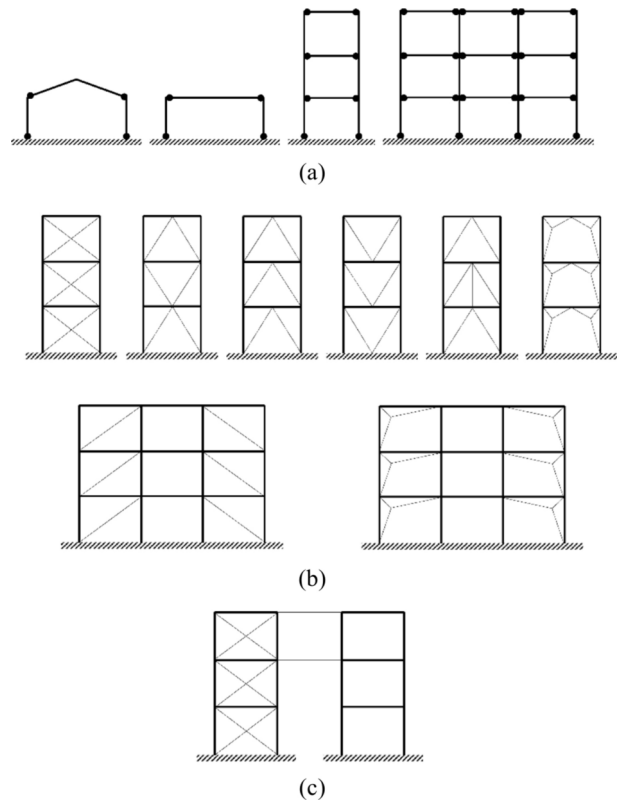
# 1 Introduction

Materials referred to as 6000 series aluminium alloys are termed structural alloys and have various performance characteristics that make them very attractive for moment resisting and braced frame structures (e.g., Georgantzia et al. 2021a). The ability of aluminium alloys to be extruded into any bespoke shape offers design flexibility allowing to place the material where it is most needed and thus minimising material waste. Thus, the power of the ‘put-the-metal-where-you-need-it’ flexibility can result in significant benefits in manufacturing cost and energy consumption aligning with sustainable practices (see the recent review by Georgantzia and Kashani (2024)). Aluminium alloys are durable, as they rapidly form a thin protective oxide layer on their surface that gives them excellent resistance to corrosion in mild environments (Georgantzia and Kashani 2024). Aluminium alloys also offer superior low-temperature toughness and thus eliminate concerns about brittle fracture, even in severe weather e.g. in cold regions (Das and Kaufman 2007). The density of aluminium alloys is about  $2.7 \text{ g/cm}^3$ , about a third of that of steel (Mazzolani 2004). In seismic prone design where the mass is a concern, aluminium alloys (unlike steel) can satisfy the required strength and ductility requirements without a weight penalty (see Georgantzia et al. 2023 and Georgantzia and Kashani 2023). The high strength-to-weight ratio minimises the total weight of the superstructure and thus reduces the substructure costs, which is particularly beneficial in poor ground conditions or where existing substructures are to be reused. Typical structural systems are shown in Fig. 1, for aluminium alloy buildings.

Various published studies have presented results that improve confidence in the prediction of structural behaviour and the assessment of codification rules of aluminium alloy frame structural components, i.e., beams, columns, connections and joints (see the first author’s doctoral thesis Georgantzia 2022) for more details on reviews of these research studies). Bock et al. (2021) reported testing on square hollow sections (SHSs) and rectangular hollow sections (RHSs) subjected to biaxial bending. Bock et al. (2021) compared the obtained experimental results with the estimations according to the design code EN 1999-1-1 (British Standards Institution 2010). This comparison revealed that EN 1999-1-1 (British Standards Institution 2010) underestimated, by about 17%, the biaxial bending resistance. The numerical study of Piluso et al. (2019) investigated the ultimate response of H- and I-sections subjected to non-uniform bending. The authors used these results to calibrate empirical formulations for estimation of rotation capacity and ultimate bending resistance of such sections (Piluso et al. 2019). Georgantzia et al. (2022a) reported an experimental and numerical programme to investigate C-section minor axis bending behaviour. A design method was also suggested for slender C-sections under minor axis bending based on the plastic effective width concept (Georgantzia et al. 2022a). This new method allows the inelastic reserve capacity in line with the results reported in Georgantzia et al. (2022a). Georgantzia et al. (2022b) then tested two-span continuous beams made from 6082-T6 RHSs to investigate the possibility for moment redistribution. The test data showed that there was the enough rotational capacity and capability for moment redistribution (Georgantzia et al. 2022b).

Georgantzia et al. (2023) examined the flexural buckling behaviour of 6082-T6 C-sections and suggested a new flexural buckling curve for EN 1999-1-1 (British Standards Institution 2010). This new curve was shown to improve the design accuracy by about 5% (Georgantzia et al. 2023). Oyeniran Adeoti et al. (2015) reported on the reliability of present design rules on 6082-T6 H-section and RHS columns. Zhu and Young (2006) numerically

**Fig. 1** Typical aluminium alloy structural systems; **a** moment-resisting frames, **b** concentrically braced frames and **c** dual frames



investigated the stability of RHSs and SHSs columns (with and without transverse welds). Georgantzia et al. (2021b) reported comprehensive experimental and numerical work which investigated the flexural buckling performance of aluminium tubular columns (filled with concrete and unfilled with concrete). The results from (Georgantzia et al. 2021b) revealed that the concrete infill delays buckling and therefore the tubular columns (concrete-filled) demonstrated higher strength and stiffness than the unfilled columns. Gkantou et al. (2023) suggested the combination of structural aluminium alloys with low carbon geopolymer concrete to manufacture structural members with lower embodied carbon. In this study, 6082-T6 SHSs were tested under uniform compression after infilling with geopolymer concrete (Gkantou et al. 2023). In addition, these cross-sections were tested after infilling with ordinary Portland cement (OPC) concrete (Gkantou et al. 2023). The results demonstrated that filling the aluminium tubes with geopolymer concrete gives equal performance compared to those filled with OPC concrete and therefore, in composite aluminium-concrete sections replacement of the concrete infill with the more sustainable geopolymer concrete infill can be done without significantly affecting the ultimate section strength (Gkantou et al. 2023).

Kim (2012) performed tests on bolted connections (single-shear) and showed the curling effect sharply reduced the ultimate capacity. Following these findings, Cho and Kim (2016) modified the strength equations to consider the curling effect for both the bearing factor and for also for block shear fracture. Guo et al. (2015, 2016) reported tests on fourteen aluminium alloy gusset joints to investigate out-of-plane flexural response. These results were

utilised to develop simplified design equations to estimate local buckling and resistance against block tearing (Guo et al. 2015, 2016). Guo et al. (2018) studied the flexural response of aluminium alloy gusset joints subjected to temperatures up to 300 °C and offered design criteria for non-linear flexural stiffness and bearing capacity.

In moment resisting and/or braced frame structures subject to earthquake loading the dissipative members form plastic hinges with large rotational demands and thereby are subjected to significant cyclic strain deformations (Tremblay et al. 2003; Stojadinovic 2003; Uriz 2005; Kashani et al. 2019; Afsar Dizaj and Kashani 2022). These strains can cause local fracture due to low-cycle fatigue (LCF). Within the plastic hinge local buckling may reduce fatigue life due to increasing local strain within the hinge (Ikeda and Mahin 1986). Upon the initiation of fracture, the deterioration of the entire element under cyclic loading is generally rather rapid (Ikeda and Mahin 1986; Ge et al. 2020; Afsar Dizaj and Kashani 2020). The seismic performance of frame structures depends on the performance of dissipative elements, which is purely governed by plastic hinge deformations in beams, columns, or braces (Uriz 2005; Lima and Martinelli 2019; Hammad and Moustafa 2021; Bai et al. 2021). Fracturing of such elements leads to strength and stiffness degradation, which requires the development of a potentially new and unanticipated loading path thus changing the response of structure under earthquake dynamic loading and this will significantly affect the maximum displacements exhibited by a braced frame structure under significant earthquake loading (Ikeda and Mahin 1986). Therefore, the effect of LCF is an essential phenomenon to be captured when modelling aluminium alloy braced frames.

There is a significant paucity of literature in investigating LCF behaviour of 6000 series aluminium alloys. Yahya et al. (2015) studied the influence of strain rate and amplitude on the LCF behaviour of 6063-T6 alloy by conducting tests at constant strain rate up to 1% strain amplitude. Fatigue life was shown to decrease with increase in strain amplitude and reducing loading frequency. Borrego et al. (2004) performed LCF tests on 6063-T6 and 6060-T6 alloys subjected to strain ranges between 0.32% and 4%. Borrego et al. (2004) used Morrow's local stress and strain approach (Morrow 1968) to estimate strain–fatigue life. Xiang et al. (2017) performed 15 ultra-LCF tests on double-edge notched coupons made from 6061-T6 alloy and suggested a fracture model which accounts for different accumulating rates of isotropic and kinematic hardening correlated damage. Pisapia et al. (2023) tested 6060-T4, 6060-T6 and 6082-T6 alloys under LCF loading and found that the 6060-T4 and 6060-T6 alloys exhibited higher cyclic hardening behaviour compared to the 6082-T6 alloy tested.

Based on the above literature review, it is evident that there are no available methods for predicting the LCF behaviour of 6000 series aluminium alloys. This study focuses on calibrating a LCF life model for use in conjunction with the modified Giuffrè-Menegotto-Pinto (GMP) model recently proposed by Georgantzia et al. (2024) for simulating the behaviour of aluminium alloy structures in the open-source Open System for Earthquake Engineering Simulation (OpenSees) software (OpenSees 2011). The GMP model (Giuffrè 1970; Menegotto and Pinto 1973) is a uniaxial nonlinear hysteretic constitutive model originally developed for carbon steel and particularly for reinforcing steel bars in structural concrete and steel sections and the model has been implemented in OpenSees (OpenSees 2011). Recently, Georgantzia et al. (2024) modified the GMP model to accurately predict the non-linear cyclic behaviour of 6082-T6, 6063-T6 and 6060-T5 aluminium alloys. However, as was explained above, when members subjected to large deformations under cyclic load-

ing, fatigue can significantly affect their structural performance. Therefore, fatigue must be considered and used to predict the onset of fracture when modelling structures under cyclic loading. To this end, an experimental programme involving 18 low-cycle high amplitude fatigue tests were conducted at the University of Bristol to establish strain–life relationships for 6082-T6, 6063-T6 and 6060-T5 aluminium alloys (using some of the methodology outlined in Georgantzia et al. (2024)). The experimental results were utilised to model the low-cycle high amplitude fatigue life and behaviour of the studied alloys. The comparison of the experimental results and predicted fatigue behaviour denotes the capability of the proposed material model to predict to a high degree of precision the onset of fracture and the overall fatigue behaviour of material. Furthermore, it is demonstrated how this model can be used in the OpenSees (OpenSees 2011) in conjunction with the GMP model to simulate the nonlinear behaviour of aluminium components subject to cyclic loading.

## 2 Tested aluminium alloys and summary of monotonic tensile testing

### 2.1 Engineering properties of the studied aluminium alloys

The manufacture and fabrication process for 6000 series alloys is discussed in detail in (Georgantzia et al. 2024). The commonly used 6082-T6, 6063-T6 and 6060-T5 alloys were selected to be investigated in this study with manufacturer reported chemical composition from (Aalco 2022). Table 1 shows the chemical compositions of the studied materials. The manganese added in the new strong 6082-T6 alloy has significant influence on the grain structure. The ‘structural alloy’ 6082-T6 is mostly used in high stress structural scenarios as a replacement for the older 6061-T6 alloy. Nonetheless, the surface finish is rougher than that of the 6063-T6 and 6060-T5 alloys and thus it is challenging to produce complex extruded cross-sections. The ‘architectural alloys’ 6063-T6 and 6060-T5 have higher strength and are suited for welding and are often used for complex extrusions for use in building applications.

**Table 1** Nominal chemical composition of the examined aluminium alloys (original data from aalco (2022)) (table adapted from Georgantzia et al. (2024)) [Used with permission of American Society of Civil Engineers, from: Journal of Materials in Civil Engineering, E. Georgantzia et al., vol. 36 no. 6, 2024; permission conveyed through Copyright Clearance Center, Inc.]

	Aluminium Alloy		
	6082-T6	6063-T6	6060-T5
Element	% Present		
Silicon (Si)	0.70–1.30	0.20–0.60	0.30–0.60
Magnesium (Mg)	0.60–1.20	0.45–0.90	0.35–0.60
Manganese (Mn)	0.40–1.00	0–0.10	0–0.10
Iron (Fe)	0–0.50	0–0.35	0.10–0.30
Chromium (Cr)	0–0.25	0–0.10	0–0.05
Zinc (Zn)	0–0.20	0–0.10	0–0.15
Titanium (Ti)	0–0.10	0–0.10	0–0.10
Copper (Cu)	0–0.10	0–0.10	0–0.10
Others (Each)	0–0.05	0–0.05	0–0.05
Others (Total)	0–0.15	0–0.15	0–0.15
Aluminium (Al)	Balance	Balance	Balance

## 2.2 Monotonic tensile tests (Georgantzia et al. 2024)

Georgantzia et al. (2024) investigated stress–strain response of 6082-T6, 6063-T6 and 6060-T5 aluminium alloys by conducting nine monotonic tensile tests. Three coupon specimens were tested under monotonic tensile loading for each considered alloy. The coupons were cut from the flat faces of 3.3 mm thick hollow sections and machined to the BS EN ISO 6892-1 (British Standards Institution 2009) standard and then loaded (monotonic tensile) at 0.2 mm/min up to fracture. All tested coupons experienced necking close to the fracture section and failed in a ductile manner. The material properties from the experiments are summarised in Table 2. The strain hardening ratio  $\sigma_u/\sigma_{0.2}$  is also given in Table 2. The strain hardening behaviour appears to be more pronounced in the 6082-T6 aluminium alloy with  $\sigma_u/\sigma_{0.2}=112\%$ . The coupon specimens were designated using the type of aluminium alloy and the test number. For instance, the label ‘6082-T6-1’ indicates a coupon specimen fabricated from 6082-T6 aluminium alloy which tested ‘first’ under monotonic tensile loading. Figure 2 shows the experimentally obtained stress–strain ( $\sigma$ – $\varepsilon$ ) curves. The three studied alloys have around 98% of their average alloy composition in common. However, the 6082-T6 alloy may have less percentage of Fe compared to 6063-T6 and 6060-T5 alloys and thus it exhibited lower  $\sigma_{0.2}$  and  $\sigma_u$  but higher  $\varepsilon_f$ .

**Table 2** Material properties obtained from monotonic tensile tests (table adapted from Georgantzia et al. (2024)) [Used with permission of American Society of Civil Engineers, from: Journal of Materials in Civil Engineering, E. Georgantzia et al., vol. 36 no. 6, 2024; permission conveyed through Copyright Clearance Center, Inc.]

Specimen	$E$ (MPa) <sup>a</sup>	$\sigma_{0.1}$ (MPa) <sup>b</sup>	$\sigma_{0.2}$ (MPa) <sup>c</sup>	$\sigma_u$ (MPa) <sup>d</sup>	$\varepsilon_u$ (%) <sup>e</sup>	$\varepsilon_f$ (%) <sup>f</sup>	$n^g$	$\sigma_u/\sigma_{0.2}$ (%)
6082-T6-1	66,638	258.2	263.9	296.0	9.18	13.68	31.84	112
6082-T6-2	60,182	259.8	266.6	299.2	7.93	16.13	26.95	112
6082-T6-3	73,081	260.6	268.8	301.5	8.43	13.50	22.40	112
6063-T6-1	66,323	322.0	325.2	336.6	6.99	11.39	69.37	103
6063-T6-2	62,716	322.9	325.9	337.2	7.50	12.60	74.72	103
6063-T6-3	63,488	322.8	325.8	337.5	6.90	12.05	75.66	104
6060-T5-1	67,434	302.0	306.2	315.7	6.80	9.44	50.79	103
6060-T5-2	64,862	301.5	306.0	315.9	6.79	9.38	46.69	103
6060-T5-3	65,094	302.4	305.9	315.3	7.34	11.32	60.69	103

<sup>a</sup>initial modulus of elasticity

<sup>b</sup>0.1% proof stress

<sup>c</sup>0.2% proof (yield) stress

<sup>d</sup>the ultimate tensile stress

<sup>e</sup>strain corresponding to ultimate tensile stress

<sup>f</sup>strain at fracture

<sup>g</sup>strain hardening exponent (Ramberg and Osgood 1943; Hill et al. 1960)



**Fig. 2** Stress–strain curves obtained from the monotonic tensile tests (plot adapted from Georgantzia et al. (2024)) [Used with permission of American Society of Civil Engineers, from: Journal of Materials in Civil Engineering, E. Georgantzia et al., vol. 36 no. 6, 2024; permission conveyed through Copyright Clearance Center, Inc.]

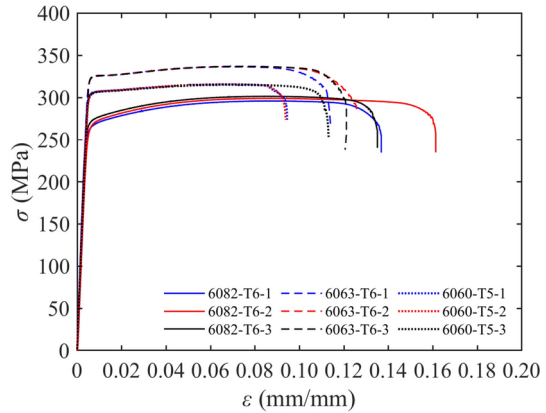
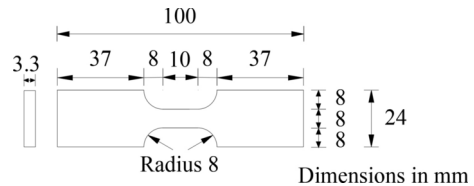


**Fig. 3** Geometry of coupon specimens (adapted from Georgantzia et al. (2024)) [Used with permission of American Society of Civil Engineers, from: Journal of Materials in Civil Engineering, E. Georgantzia et al., vol. 36 no. 6, 2024; permission conveyed through Copyright Clearance Center, Inc.]



### 3 Low-cycle high amplitude fatigue tests

The new experiments reported in this paper were performed in the Heavy and Light Structures Laboratory at the University of Bristol in the UK. In total, 18 low-cycle high amplitude fatigue tests were conducted (up to  $\pm 6\%$  strain amplitude) to establish strain – life relationships for 6082-T6, 6063-T6 and 6060-T5 aluminium alloys.

#### 3.1 Geometry of test specimens

Test coupons were extracted with a waterjet cutter from the flat faces of the same hollow sections with their counterparts subjected to monotonic tensile loading. The coupons were machined to the geometric requirements described in ASTM E606-04 (ASTM International 2017) (Fig. 3). The adopted gauge length is quite small to ensure as uniform as possible distribution of strain thus preventing at the compression stage premature buckling failure.

#### 3.2 Assessment of potential failure due to buckling

Prior to the testing programme, analytical calculations were carried out to estimate the critical buckling load  $F_{cr,b}$  of the coupons and assess the possibility of failure due to buckling. The  $F_{cr,b}$  was calculated based on the double-modulus theory (Timoshenko and Gere 1961), Eq. (1):

$$F_{cr,b} = \frac{\pi^2 E_r I}{(\kappa L)^2} \quad (1)$$

where  $E_r$ =reduced modulus of elasticity given in Eq. (2),  $I$ =second moment of area of the coupons,  $L$ =length of the coupons and  $\kappa$  is the effective length factor taken as 0.5 as both ends of the coupon remain fixed during LCF testing.

$$E_r = \frac{4E_m E_t}{(\sqrt{E_m} + \sqrt{E_t})^2} \quad (2)$$

where  $E_m$  and  $E_t$  are the Young's and tangent modulus, respectively, taken as average values of those obtained from the monotonic tensile tests and for all coupons made from the same alloy. The buckling length  $L$  and theoretical  $F_{cr,b}$  values for the coupons for each examined aluminium alloy are listed in Table 3. The same table also includes the ultimate loads  $F_u$  calculated using the average ultimate stresses  $\sigma_u$  obtained from the monotonic tensile tests. The  $F_{cr,b}$  values are quite higher than the corresponding  $F_u$  values indicating no potential failure due to buckling during LCF testing.

### 3.3 Test setup and loading protocol

Upon machining, each coupon was set between the hydraulic wedge grips of a 250 kN INSTRON universal testing machine and tested under constant total strain amplitude rate cycles (with full reversal) up to the fracture point. As was done in (Kashani et al. 2015) an integral linear variable displacement transducer was used for measurement of the displacement of the machine grips. Due to small gauge length of the coupons, it was not feasible in this study to apply an extensometer or a strain gauge to measure the developed strains. Hence, the measured displacement values of the machine grips were converted into strains similar to the study of Kashani et al. (2015). Figure 4 illustrates the LCF test setup. The experiments were conducted with displacement control with zero mean strain utilising a sine wave loading pattern (constant amplitude) as was done in (Kashani et al. 2015). The strain rate was  $5 \times 10^{-3} \text{ s}^{-1}$  following BS 7270 (British Standards Institution 2006) so that the generated heat did not significantly affect the results. LCF tests were carried out at  $\pm 1\%$ ,  $\pm 2\%$ ,  $\pm 3\%$ ,  $\pm 4\%$ ,  $\pm 5\%$  and  $\pm 6\%$  strain amplitudes, which allowed for significant plastic deformation covering the LCF regime. One coupon specimen was tested at each strain amplitude for each examined aluminium alloy resulting in total 18 LCF tests.

## 4 Experimental results and discussion

The results obtained from the low-cycle high amplitude fatigue tests are summarised in Table 4 including strain amplitude  $\varepsilon_{ap}$ , total time, frequency, and number of half cycles to failure  $2N_f$ . As anticipated, crack initiation induced due to fatigue was quicker with strain amplitude increase. Figure 5 shows three fractured coupon specimens after LCF testing at  $\pm 5\%$  strain amplitude. Figures 6 and 7 present the normalised hysteretic responses at  $\pm 4\%$  and  $\pm 6\%$  strain amplitudes, respectively, for all the studied aluminium alloys. It should be

**Table 3** Assessment of potential failure due to buckling

Aluminium alloy	$L$ (mm)	$F_{cr,b}$ (kN)	$F_u$ (kN)
6082-T6	10.0	21.2	7.9
6063-T6	10.0	14.4	8.9
6060-T5	10.0	17.0	8.3

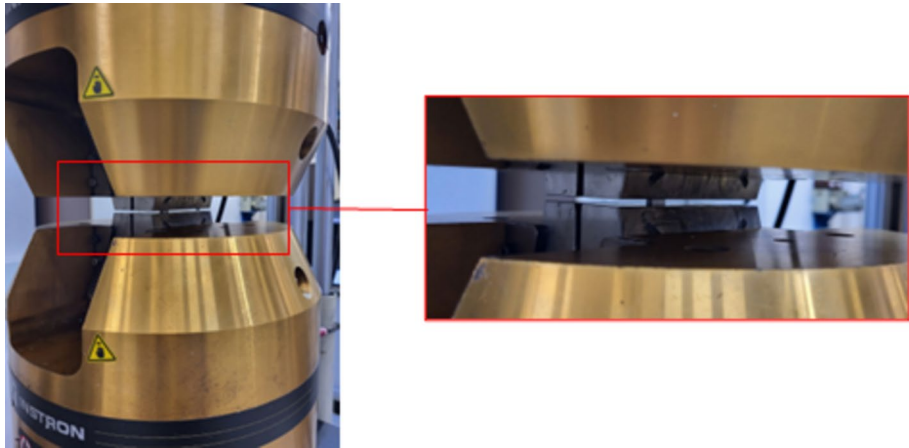


**Fig. 4** LCF test setup (photo: authors)

**Table 4** LCF test results

Strain amplitude $\varepsilon_{ap}$	Total time (s)	Frequency (Hz)	Number of half cycles to failure $2N_f$
<i>6082-T6</i>			
$\pm 1\%$	86,571.6	0.125	21,643
$\pm 2\%$	2615.2	0.063	327
$\pm 3\%$	1342.3	0.042	112
$\pm 4\%$	586.2	0.031	37
$\pm 5\%$	495.9	0.025	25
$\pm 6\%$	408.0	0.021	17
<i>6063-T6</i>			
$\pm 1\%$	92,808.4	0.125	23,202
$\pm 2\%$	3045.5	0.063	381
$\pm 3\%$	1543.9	0.042	129
$\pm 4\%$	758.1	0.031	47
$\pm 5\%$	792.2	0.025	40
$\pm 6\%$	531.8	0.021	22
<i>6060-T5</i>			
$\pm 1\%$	100,706.0	0.125	25,177
$\pm 2\%$	3525.6	0.063	441
$\pm 3\%$	947.2	0.042	79
$\pm 4\%$	508.0	0.031	32
$\pm 5\%$	321.4	0.025	16
$\pm 6\%$	203.1	0.021	8

noted that in Figs. 6 and 7 tension is positive, and compression is negative. The three alloys exhibited similar strain–life behaviours while noting the varying elongations at fracture observed in the monotonic tensile tests (see Fig. 2). This may be attributed to the fatigue life at high strain amplitudes being proportional to  $\sigma_u$  and  $\varepsilon_f$  (Manson and Hirschberg 1970).

**Fig. 5** Fractured coupon specimens after LCF testing at  $\pm 5\%$  strain amplitude (photo: authors)

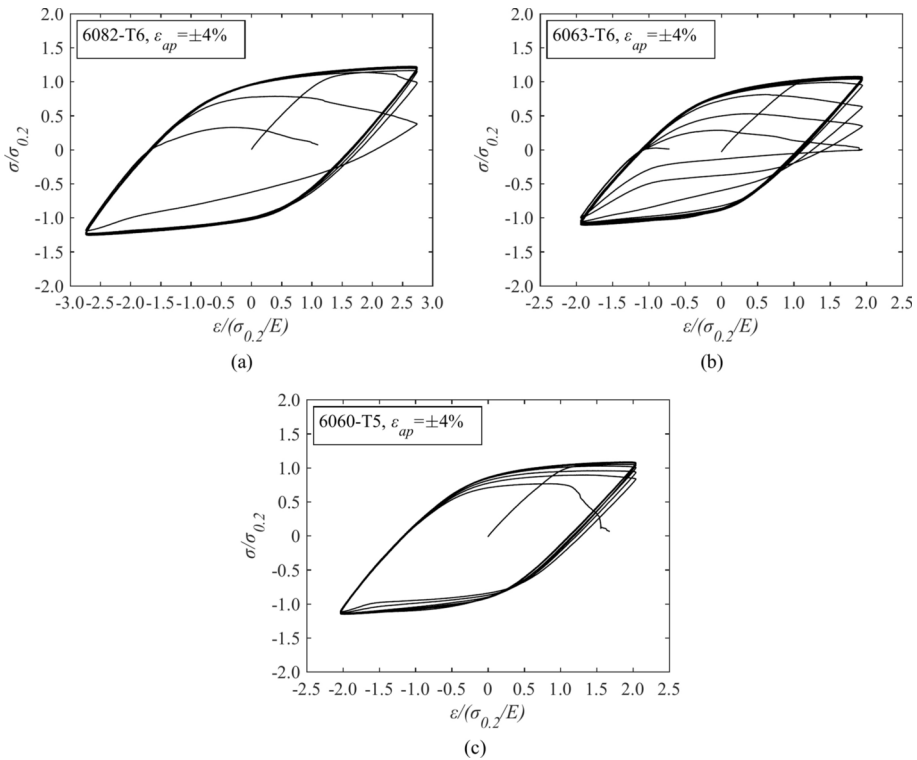
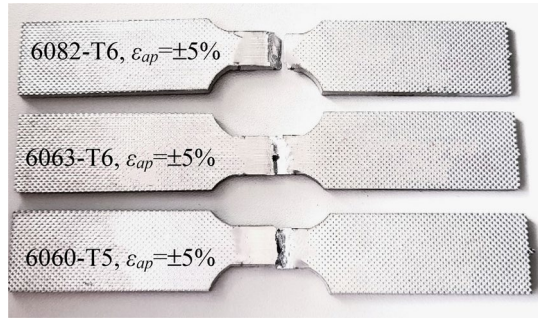


**Fig. 6** Normalised hysteretic response of the examined aluminium alloys at 4% strain amplitude

The 6082-T6 alloy exhibited the highest average  $\varepsilon_f$ , however the higher average  $\sigma_u$  of 6063-T6 and 6060-T5 alloys compensated for their lower average  $\varepsilon_f$  and thus the three alloys exhibited similar strain–life behaviour. Moreover, the hysteretic responses at both applied strain amplitudes appear to be almost symmetric in tension and compression. The hysteretic loops for all studied aluminium alloys are relatively plump implying adequate energy dissipation capacity. The small gauge length prevented buckling occurrence and thus there was no strength degradation before the end of the tests. As the strain demand increased past yield, a kinematic combined with marginal isotropic hardening behaviour was revealed until

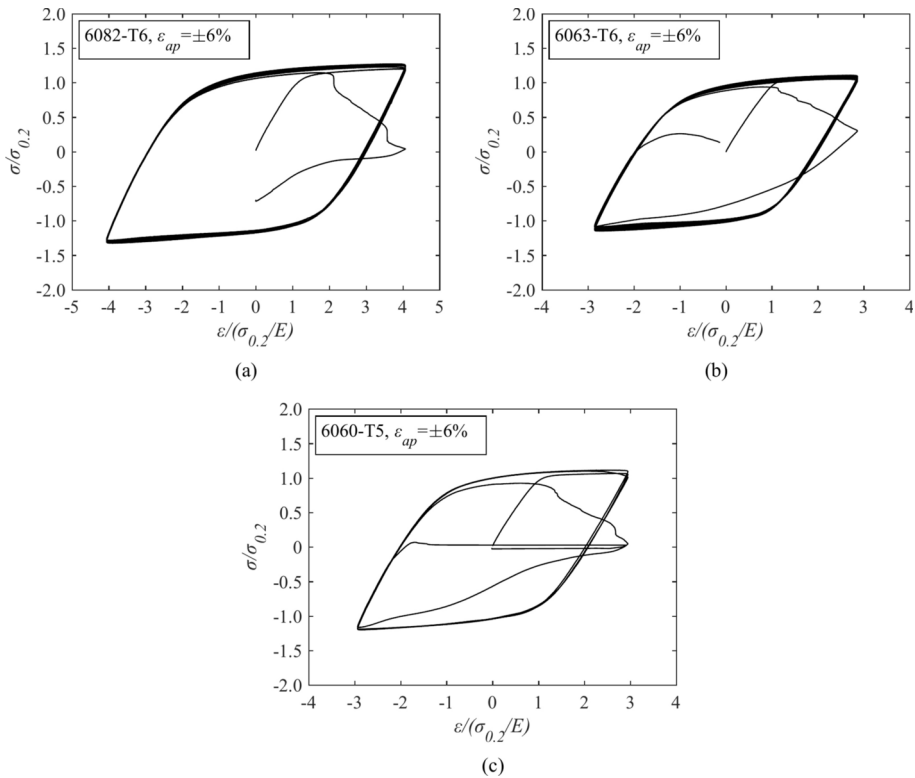


**Fig. 7** Normalised hysteretic response of the examined aluminium alloys at 6% strain amplitude

the maximum stress was reached (as also observed in Georgantzia and Kashani (2023) and Georgantzia et al. (2024)).

## 5 Analytical modelling

### 5.1 Low-cycle high amplitude fatigue life of 6000 series aluminium alloys

There are three methods often used to model the LCF life of aluminium alloys, i.e., Coffin-Manson (Coffin 1954; Manson 1965), Koh-Stephens (Koh and Stephens 1991) and Energy Method (Chang and Mander 1994). These methods can only be applied for LCF under loading of constant amplitude. However, earthquake actions are uncertain in terms of their time and frequency of occurrence. Hence, Miner's rule (Miner 1945) was applied to capture the cumulative damage as a result of random loading history (see Brown and Kunnath 2000; Kunnath et al. 2009; Kashani et al. 2013) for further discussion).

The Coffin-Manson (Coffin 1954; Manson 1965) and Koh-Stephens (Koh and Stephens 1991) models are mostly used by structural engineering researchers as they can be easily implemented in finite element analysis to analyse civil engineering structures subjected to seismic loading (e.g. OpenSees (OpenSees 2011)). Both Coffin-Manson (Coffin 1954;

Manson 1965) and Koh-Stephens (Koh and Stephens 1991) models employ a strain life approach for predicting the LCF life materials. The most significant parameter influencing the LCF life of a material is the plastic strain amplitude  $\varepsilon_p$ . Thus, Coffin-Manson (Coffin 1954; Manson 1965) model relates  $\varepsilon_p$  to the fatigue life as described in Eq. (3) (also used in Filippou et al. (1983)):

$$\varepsilon_p = \varepsilon'_f (2N_f)^c \quad (3)$$

where  $\varepsilon'_f$ =the ductility coefficient namely the single load reversal plastic fracture strain,  $c$ =the ductility exponent and  $2N_f$ =the number of half-cycles i.e. number of load reversals to failure.

Koh and Stephens (1991) noted that for many problems related to fatigue in engineering metallic materials the plastic strain component remains constant and thus they extended the Coffin-Manson (Coffin 1954; Manson 1965) method based on the total strain amplitude  $\varepsilon_a$  (summation of elastic and plastic strains). The proposed Koh-Stephens (Koh and Stephens 1991) method is given by Eq. (4):

$$\varepsilon_a = \varepsilon_f (2N_f)^a \quad (4)$$

where  $\varepsilon_f$ =the ductility coefficient i.e. the total fracture strain for single load reversal,  $a$ =the ductility exponent.

During the experiments the total strain amplitudes were held constant and the amplitudes of the elastic and plastic strain components did not change. This is because cyclic hardening of the material was transient, and the behaviour stabilised quickly, as shown by Fig. 8: see the  $\sigma$  and  $\varepsilon$  measurements from the first eight cycles of the  $\pm 4\%$  strain amplitude test of the 6082-T6 aluminium. Therefore, in this research, the Koh-Stephens model (Koh and Stephens 1991) was used to predict the LCF life of the studied aluminium alloys. Equation (4) was fitted to the obtained experimental results for each studied aluminium alloy to calibrate  $\varepsilon_f$  and  $a$ . The results from fatigue tests at  $\pm 1\%$  strain amplitude were not utilised as they do not represent the number of cycles that a structure could experience during seismic events. The regression analysis outputs are given in Table 5 and Fig. 9 shows Eq. (4) fitted to the

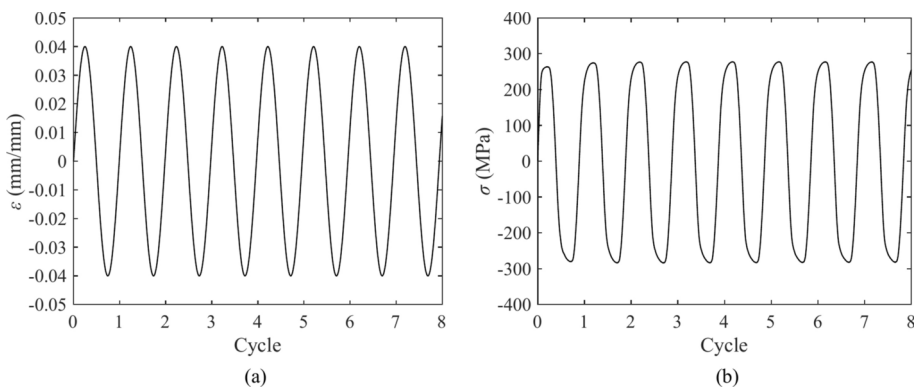


**Fig. 8** Measurements of **a** strain and **b** stress during the first few cycles of the  $\pm 4\%$  strain amplitude test of the 6082-T6 aluminium

**Table 5** Results of regression analysis to calibrate the Koh-Stephens model (Koh and Stephens 1991) parameters

Aluminium alloy	$\varepsilon_f$	$\alpha$	Coefficient of determination $R^2$	No. of data points in the regression analysis	$p$ -value
6082-T6	0.168	-0.375	0.981	5	0.0016
6063-T6	0.204	-0.397	0.973	5	0.0009
6060-T5	0.112	-0.293	0.997	5	0.0002

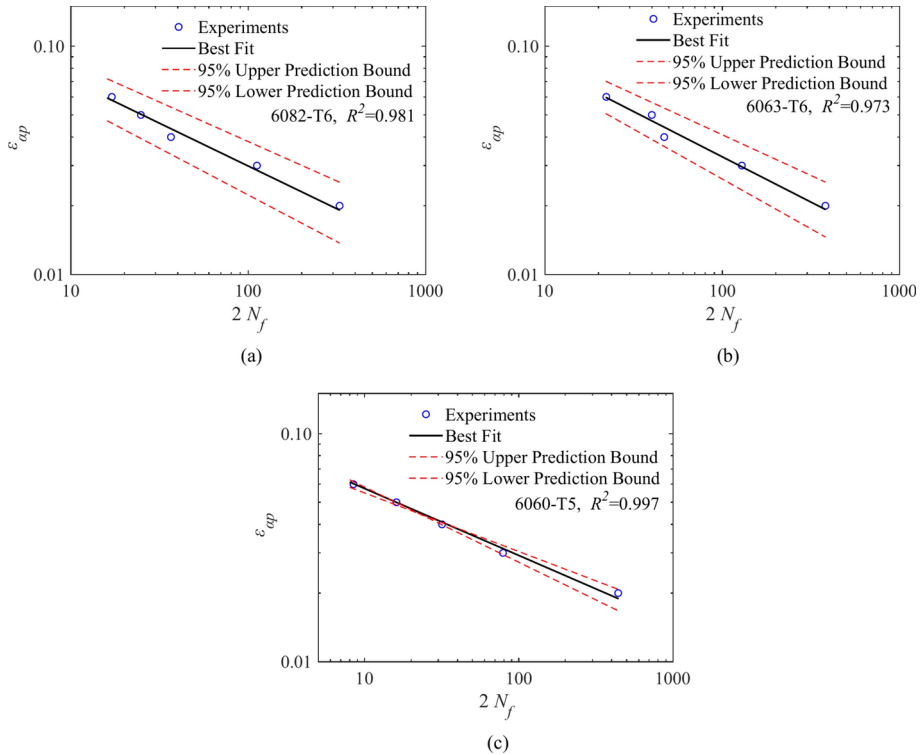


**Fig. 9** Calibration of Koh-Stephens model (Koh and Stephens 1991) parameters for all studied aluminium alloys (No. of data points used in the regression=5)

experimental results for the studied aluminium alloys using nonlinear regression analysis in MATLAB (version 2022b) (The MathWorks Inc. 2022).

## 5.2 Low-cycle high amplitude fatigue behaviour of 6000 series aluminium alloys

A fibre element modelling technique has been developed in OpenSees software (OpenSees 2011). Particularly, beam elements are used to build the model and the section is broken down into fibres where uniaxial materials are defined independently (see Spacone et al. 1996a, b). The coupled flexural and axial stiffnesses/strength are calculated by integrating strains across the section (see Spacone et al. 1996a,b). Fibre element modelling has low computational cost, is a relatively simple modelling approach, and has reasonable accuracy

as reported by other researchers (e.g., Spacone et al. 1996a,b; Uriz 2005; Kashani et al. 2018).

The Giuffrè-Menegotto-Pinto (GMP) model (Giuffrè 1970; Menegotto and Pinto 1973) is a uniaxial nonlinear hysteretic constitutive model for carbon steel implemented into OpenSees (OpenSees 2011) as the *Steel02* command. As described in Georgantzia et al. (2024) this model consists of 10 time-invariant material parameters: initial Young's modulus  $E_0$ , yield stress  $\sigma_{0.2}$ , post-yield hardening ratio  $b$ , initial curvature between elastic and post-yield slope  $R_0$ , curvature variation parameter of Bauschinger curve after each strain reversal  $cR_1$ , curvature variation parameter of Bauschinger curve after each strain reversal  $cR_2$ , isotropic hardening parameters defining stress shift in compression  $\alpha_1$  and  $\alpha_2$ , and isotropic hardening parameters defining stress shift in tension  $\alpha_3$  and  $\alpha_4$  (see Georgantzia et al. (2024) for more details). Recently, Georgantzia et al. (2024) performed monotonic and cyclic coupon tests up to 6.5% strain amplitude and modified this model to extend its application on 6000 series aluminium alloys. Table 6 summarises the material parameters of the modified GMP model.

OpenSees (OpenSees 2011) contains a standard fatigue material model that may be wrapped with any steel model without affecting the stress–strain state of the original material. This model captures LCF behaviour and is the uniaxial *Fatigue* material model in OpenSees (Uriz 2005; OpenSees 2011). A modified rainflow cycle counter algorithm tracks strain amplitudes. This cycle counter algorithm was employed along with the Coffin-Manson (Coffin 1954; Manson 1965) relationship and Miner's (Miner 1945) rule to describe the LCF failure. When the *Fatigue* material damage state reaches a value of 1, the stress of the parent steel material reduces to zero. The default values of the *Fatigue* material are the parameters taken from other calibrations with LCF tests on European steel sections (Ballio and Castiglioni 1995; Uriz 2005) (see also Kashani et al. (2018) for further details)).

In the present research, the *Fatigue* material with the calibrated Koh-Stephens parameters (Table 5) were used to wrap the modified GMP model proposed by Georgantzia et al. (2024) for each studied aluminium alloy. Figures 10 and 11 show the observed and predicted normalised responses at 4% and 6% strain amplitudes, respectively, for all studied aluminium alloys. Visual comparisons between the measured and predicted curves revealed that the modified GMP model (Georgantzia et al. 2024) wrapped with the calibrated *Fatigue* material accurately predicts the onset of fracture in the same cycle was observed during testing for the tests presented herein. Once fracture is reached, the model entirely removes the element and thus there is no degradation in the model. This can also be observed on Fig. 12 which shows that for both 4% and 6% strain amplitudes, once the *Fatigue* material model reached the damage level of 1.0, the stress of the 6082-T6 alloy became zero. This is important as it denotes the capability of this material model to predict the cycle at which a structural element, bracing or frame would fail, and as fibres are removed progressively from the model produce a realistic progression of failure. Therefore, it is concluded that

**Table 6** Calibrated GMP model parameters for the hysteretic stress–strain response of 6000 series alloys (adapted from Tables 3 and 4 from Georgantzia et al. (2024)). [Used with permission of American Society of Civil Engineers, from: Journal of Materials in Civil Engineering, E. Georgantzia et al., vol. 36 no. 6, 2024; permission conveyed through Copyright Clearance Center, Inc.]

Aluminium Alloy	$E_0$ (MPa)	$\sigma_y$ (MPa)	$b$	$R_0$	$cR_1$	$cR_2$	$\alpha_1$	$\alpha_2$	$\alpha_3$	$\alpha_4$
6082-T6	66,634	266	0.005	7.5	0.6	0.15	0.051	1	0.042	1
6063-T6	64,176	326	0.003	8.5	0.6	0.15	0.035	1	0.020	1
6060-T5	65,797	306	0.003	8.5	0.6	0.15	0.046	1	0.021	1



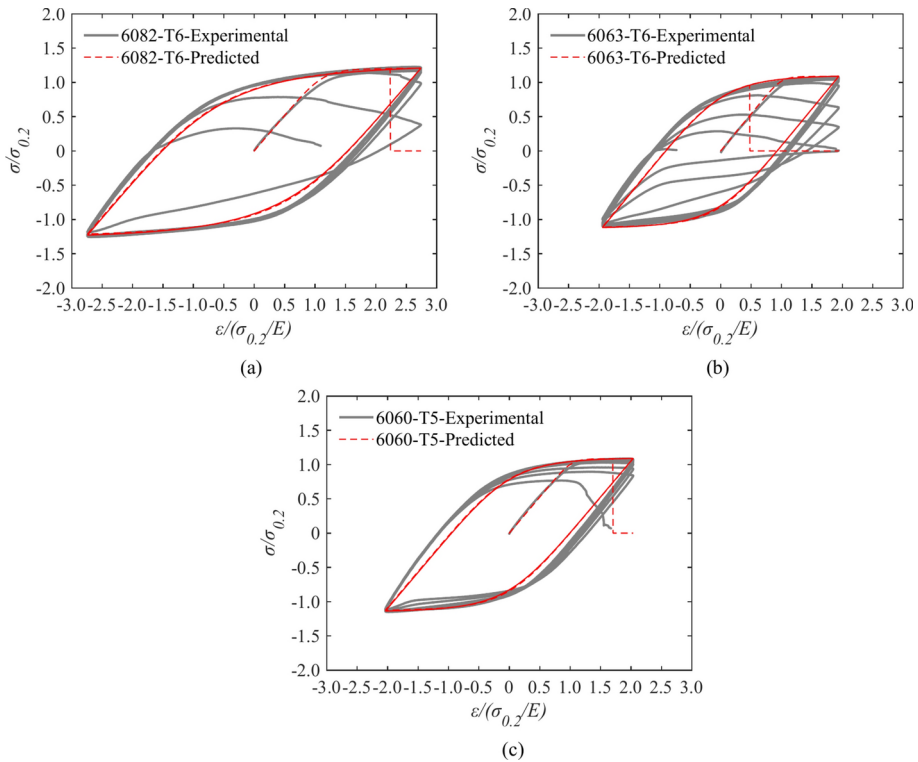


**Fig. 10** Comparison between experimental and predicted normalised responses at 4% strain amplitude for all studied aluminium alloys

the modified GMP model (Georgantzia et al. 2024) wrapped with the calibrated *Fatigue* material is capable of predicting well the fracture and fatigue life of 6000 series aluminium alloys.

## 6 Implementation of the proposed model

The modified GMP model (Georgantzia et al. 2024) wrapped with the calibrated *Fatigue* material proposed herein was implemented in OpenSees (OpenSees 2011) to model the behaviour of a hypothetical aluminium hollow section column subjected to cyclic axial loading history. A 2D non-linear model was produced as shown in Fig. 13 employing the geometric properties reported by (Georgantzia et al. 2021b). The column comprises a  $50.8 \times 50.8 \times 4.8$  SHS made from 6082-T6 aluminium alloy and is 1000 mm long with  $D$  (mm)=50.6;  $B$  (mm)=50.6;  $t$  (mm)=4.67;  $\omega_{gm}$  (mm)=0.01;  $E$  (MPa)=67,500 and  $\sigma_{0.2}$  (MPa)=305.9 (data from: Georgantzia et al. (2021b)). The *non-linearBeamColumn* element was used to build the model to account for the plasticity spread along the element length (Mazzoni et al. 2006). Pin-ended support conditions were considered, and the cyclic axial loading history was applied concentrically at the top end of the column. Hence, the top

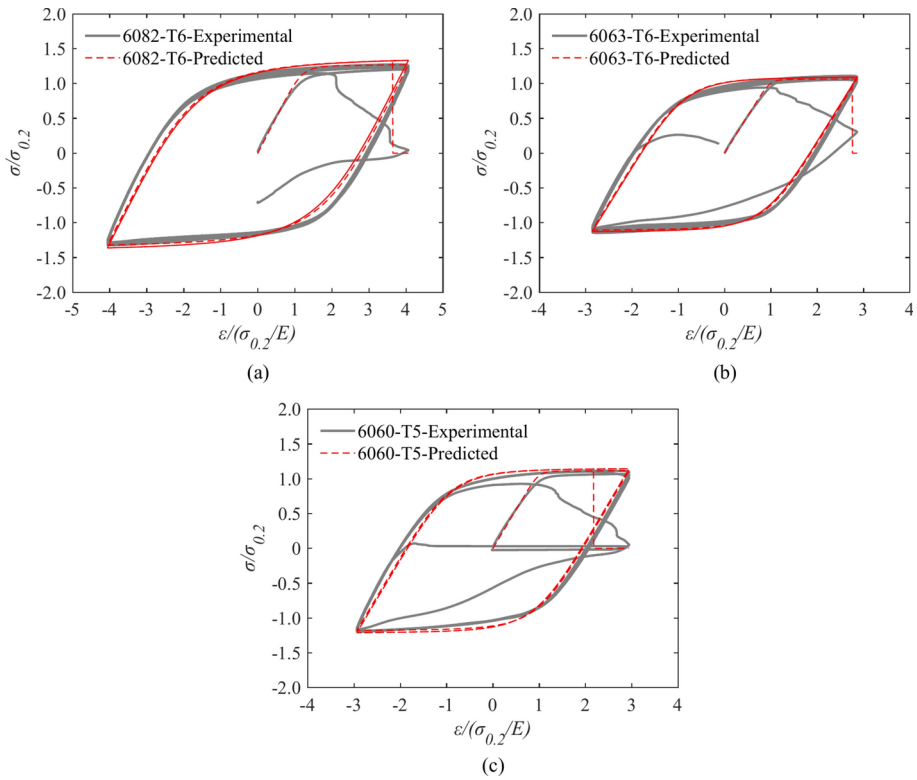


**Fig. 11** Comparison between experimental and predicted normalised responses at 6% strain amplitude for all studied aluminium alloys

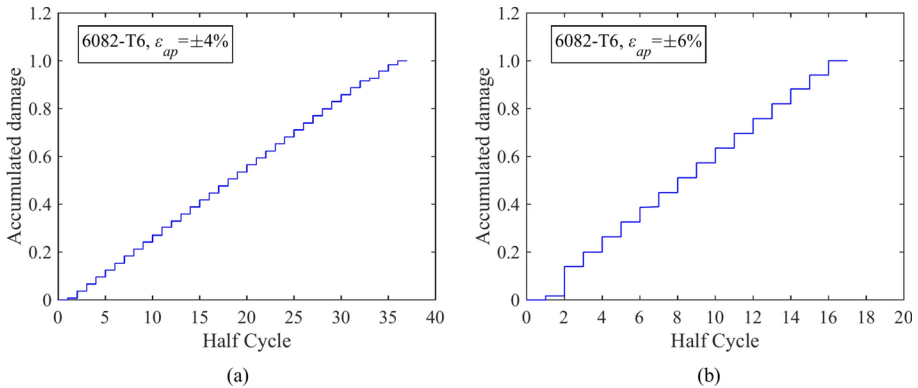


**Fig. 12** Accumulated damage at **a** 4% and **b** 6% strain amplitudes for 6082-T6 aluminium alloy

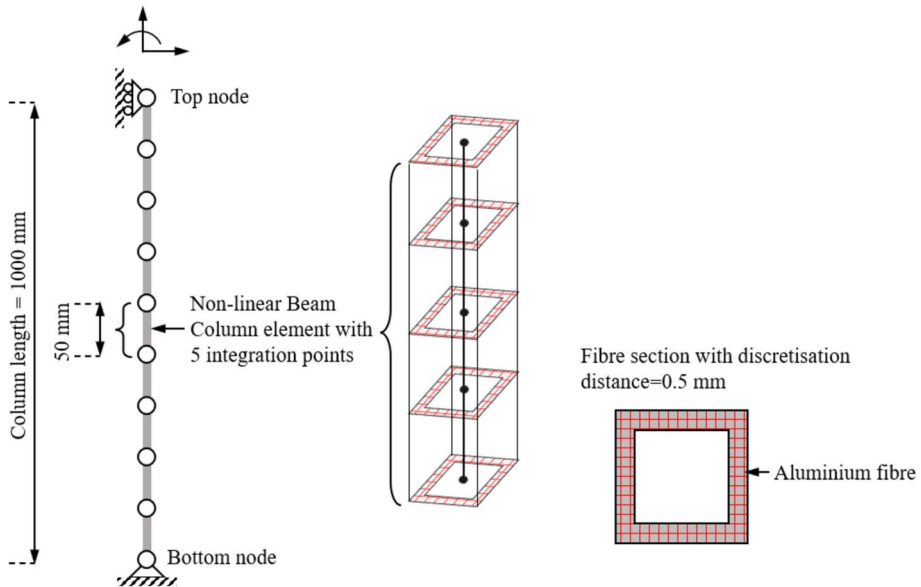


**Fig. 13** Overview of the fibre element modelling (figure adapted from (Georgantzia et al. 2024) [Used with permission of American Society of Civil Engineers, from: Journal of Materials in Civil Engineering, E. Georgantzia et al., vol. 36 no. 6, 2024; permission conveyed through Copyright Clearance Center, Inc.]

and bottom nodes were fixed against all translational degrees of freedom apart from, at the loaded end, the longitudinal translation. The rotation about the minor axis remained free.

As reported in previous studies (Georgantzia and Gkantou 2021; Georgantzia et al. 2021c, 2023), pre-existing geometric imperfections influence the structural behaviour of thin-walled members. This influence was considered by perturbing the starting geometry of the column by a Fourier sine series as described by Eq. (5) (Oyeniran Adeoti et al. 2015; Georgantzia et al. 2021c).

$$\omega_g(x)_i = \omega_{gm} \sin \frac{\pi x}{L} \quad (5)$$

where  $\omega_g$ =the global imperfection amplitude at node  $i$ ,  $\omega_{gm}$ =the maximum measured global imperfection amplitude,  $L$ =the column length and  $x$ =the distance of the node  $i$  from the bottom of the column (Fig. 14).

The global imperfection amplitude was set as 0.01 mm which was measured prior to testing. However, the initial local geometric imperfection was not considered as the formulation of the *non-linearBeamColumn element* does not easily allow the inclusion of local buckling (see Chen 2010 and Kashani 2024). The 1000 mm long column was discretised using 20 elements while a discretisation distance of 0.5 mm was employed for the fibre section. The modified GMP model (Georgantzia et al. 2024) wrapped with the calibrated *Fatigue* material was employed adopting the  $E_0$  and  $\sigma_y$  aforementioned experimental values from Georgantzia et al. (2021b) and the  $b$  and  $R_0$  values for 6082-T6 alloy from Table 6 for the analysis presented in this paper. The residual stresses caused by the heat-treatment of the 6082-T6 alloy, are neglected as they do not significantly affect the structural behaviour of

**Fig. 14** Schematic of initial global imperfections of a pin-ended column (figure adapted from (Georgantzia et al. 2024) [Used with permission of American Society of Civil Engineers, from: Journal of Materials in Civil Engineering, E. Georgantzia et al., vol. 36 no. 6, 2024; permission conveyed through Copyright Clearance Center, Inc.]

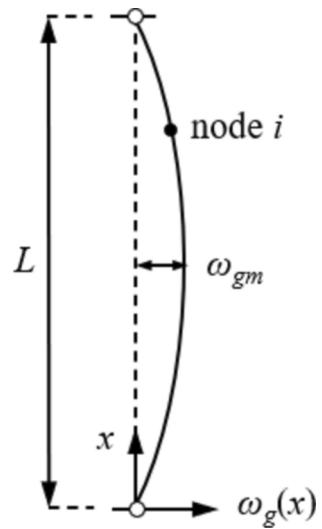
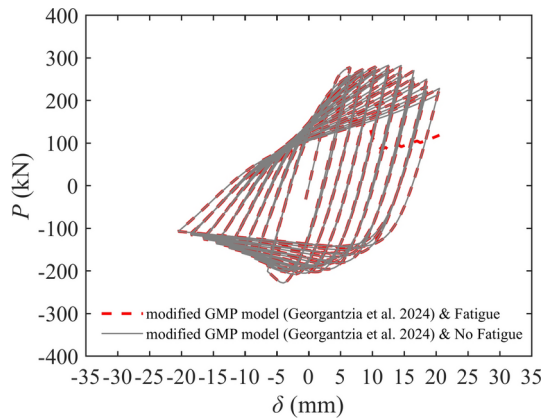


**Fig. 15** Behaviour of  $50.8 \times 50.8 \times 4.8$  aluminium hollow section column under cyclic axial loading



the elements (Mazzolani 1975). A three-cycle reversed symmetrical displacement history up to 20 mm was applied at the top node of the column. The same column was also analysed considering the modified GMP model (Georgantzia et al. 2024) without wrapping it with the now calibrated *Fatigue* material to determine the LCF influence on the column response.

Figure 15 illustrates the obtained load–axial displacement ( $P$ – $\delta$ ) curves for the  $50.8 \times 50.8 \times 4.8$  aluminium hollow section column using the modified GMP model (Georgantzia et al. 2024) wrapped with the calibrated *Fatigue* material and the modified GMP model (Georgantzia et al. 2024) without wrapping it with the calibrated *Fatigue* material. The comparison between the two curves of the hypothetical column shows that degradation due to LCF significantly affects the inelastic behaviour of aluminium hollow section columns and thereby the energy dissipation capacity of the entire structure during large earthquakes.

## 7 Summary and conclusions

A total of 18 LCF tests with amplitudes ranging from  $\pm 1\%$  to  $\pm 6\%$  were carried out to establish strain–life relationships for 6082-T6, 6063-T6 and 6060-T5 aluminium alloys. The results showed that the three considered alloys exhibited similar strain–life relationships despite the different specimen elongations at the fracture point as observed in monotonic tensile tests. It was also observed that when the strain demand increased past the yield strain, a kinematic combined with marginal isotropic hardening behaviour was detected until the maximum stress was reached. The Koh-Stephens model (Koh and Stephens 1991) was fitted to the obtained experimental results using nonlinear regression analyses to predict the LCF life of each studied aluminium alloy. Following the uniaxial *Fatigue* material in OpenSees (OpenSees 2011), the calibrated Koh-Stephens model parameters were used to wrap them to the modified GMP model proposed by (Georgantzia et al. 2024) to predict the fatigue life of the studied aluminium alloys. Comparing the experimental and predicted behaviours, it was found that the proposed material model can predict fracture onset in the same cycle. Therefore, it is currently the first (to the authors' knowledge) uniaxial material model developed for modelling the LCF life of structural aluminium alloys. As aluminium alloy braced frames have become a viable alternative, more experimental testing and numerical modelling studies are needed to provide further insights into their structural performance.

**Acknowledgements** The authors would like to thank the technicians of Heavy and Light Structures Laboratory at University of Bristol for their invaluable assistance and support.

**Author contributions** Georgantzia Evangelia: conceptualization, methodology, software, validation, formal analysis, investigation, data curation, writing-original draft, visualisation. Paul J. Vardanega: project administration, writing-review and editing. Mohammad M. Kashani: conceptualization, methodology, writing-review and editing.

**Data availability** The underlying data will be made available upon reasonable request to the first author.

## Declarations

**Competing interest** The authors declare that they have no known competing financial interests or personal relationships that could have appeared to influence the work reported in this paper.

**Open Access** This article is licensed under a Creative Commons Attribution 4.0 International License, which permits use, sharing, adaptation, distribution and reproduction in any medium or format, as long as you give appropriate credit to the original author(s) and the source, provide a link to the Creative Commons licence, and indicate if changes were made. The images or other third party material in this article are included in the article's Creative Commons licence, unless indicated otherwise in a credit line to the material. If material is not included in the article's Creative Commons licence and your intended use is not permitted by statutory regulation or exceeds the permitted use, you will need to obtain permission directly from the copyright holder. To view a copy of this licence, visit <http://creativecommons.org/licenses/by/4.0/>.

## References

- Aalco (2022) <https://www.aalco.co.uk/>. Accessed 21 Apr 2023
- Afsar Dizaj E, Kashani MM (2020) Numerical investigation of the influence of cross-sectional shape and corrosion damage on failure mechanisms of RC bridge piers under earthquake loading. Bull Earthquake Eng 18:4939–4961. <https://doi.org/10.1007/s10518-020-00883-3>

- Afsar Dizaj E, Kashani MM (2022) Influence of ground motion type on nonlinear seismic behaviour and fragility of corrosion-damaged reinforced concrete bridge piers. *Bull Earthquake Eng* 20:1489–1518. <https://doi.org/10.1007/s10518-021-01297-5>
- ASTM International (2017) ASTM E606-04: standard practice for strain-controlled fatigue testing. ASTM International, West Conshohocken
- Bai Y, Li Y, Tang Z, Bittner M, Broggi M, Beer M (2021) Seismic collapse fragility of low-rise steel moment frames with mass irregularity based on shaking table test. *Bull Earthquake Eng* 19:2457–2482. <https://doi.org/10.1007/s10518-021-01076-2>
- Ballio G, Castiglioni CA (1995) A unified approach for the design of steel structures under low and/or high cycle fatigue. *J Constr Steel Res* 34:75–101. [https://doi.org/10.1016/0143-974X\(95\)97297-B](https://doi.org/10.1016/0143-974X(95)97297-B)
- Bock M, Theofanous M, Dirar S, Lipitkas N (2021) Aluminium SHS and RHS subjected to biaxial bending: Experimental testing, modelling and design recommendations. *Eng Struct* 227:111468. <https://doi.org/10.1016/j.engstruct.2020.111468>
- Borrego LP, Abreu LM, Costa JM, Ferreira JM (2004) Analysis of low cycle fatigue in AlMgSi aluminium alloys. *Eng Fail Analysis* 11:715–725. <https://doi.org/10.1016/j.engfailanal.2003.09.003>
- British Standards Institution (2006) BS 7270 Metallic materials Constant amplitude strain controlled axial fatigue Method of test. British Standards Institution, London
- British Standards Institution (2009) BS EN ISO 6892-1-2009: The Standard for Metallic materials. Tensile testing - Method of test at ambient temperature. British Standards Institution, London
- British Standards Institution (2010) Eurocode 9: design of aluminium structures. Part 1–1: General structural rules. British Standards Institution, London
- Brown J, Kunnath SK (2000) Low Cycle Fatigue Behavior of Longitudinal Reinforcement in Reinforced Concrete Bridge Columns. Technical Report MCEER-00-0007. [https://www.buffalo.edu/mceer/catalog\\_host.html/content/shared/www/mceer/publications/MCEER-00-0007.detail.html](https://www.buffalo.edu/mceer/catalog_host.html/content/shared/www/mceer/publications/MCEER-00-0007.detail.html). Accessed Jan 01 2025
- Chang GA, Mander JB (1994) Seismic Energy Based Fatigue Damage Analysis of Bridge Columns: Part I– Evaluation of Seismic Capacity. Technical Report NCEER-94-0006. <https://www.eng.buffalo.edu/mceer-reports/94/94-0006.pdf>. Accessed Jan 01 2025
- Chen C (2010) Performance-based seismic demand assessment of concentrically braced steel frame buildings. Ph.D. thesis University of California, Berkeley, CA, USA
- Cho YH, Kim TS (2016) Estimation of ultimate strength in single shear bolted connections with aluminum alloys (6061–T6). *Thin-Walled Struct* 101:43–57. <https://doi.org/10.1016/j.tws.2015.11.017>
- Coffin Jr LF (1954) A study of the effects of cyclic thermal stresses on a ductile metal. *Transactions of ASME* 76:931–950
- Das S, Kaufman J (2007) Aluminum alloys for bridges and bridge decks. The Minerals, Metals & Materials Society Pittsburgh, PA. pp 61–72
- Filippou F, Popov E, Bertero V (1983) Effects of Bond Deterioration on Hysteretic Behavior of Reinforced Concrete Joints. DC REPORT NO. UCB/EERC-83, Washington, DC. <https://nehrpsearch.nist.gov/static/files/NSF/PB84192020.pdf>. Accessed 01 2025
- Ge X, Dietz MS, Alexander NA, Kashani MM (2020) Nonlinear dynamic behaviour of severely corroded reinforced concrete columns: shaking table study. *Bull Earthquake Eng* 18:1417–1443. <https://doi.org/10.1007/s10518-019-00749-3>
- Georgantzia E, Gkantou M (2021) Flexural buckling of concrete-filled aluminium alloy CHS columns: numerical modelling and design. In: Kumar Shukla S, Raman SN, Bhattacharjee B, Bhattacharjee J (eds) *Advances in geotechnics and structural engineering. Lecture notes in civil engineering*, vol 143. Springer, Singapore
- Georgantzia E, Kashani MM (2023) Monotonic and cyclic behaviour of 6082–T6 aluminium alloy. *ce/papers* 6(3–4):2220–2225. <https://doi.org/10.1002/cepa.2315>
- Georgantzia E, Kashani MM (2024) On the use of aluminium alloys in sustainable design, construction and rehabilitation of bridges. *Proc Inst Civ Eng Bridge Eng*. <https://doi.org/10.1680/jbrn.23.00018>
- Georgantzia E, Gkantou M, Kamaris GS (2021) Aluminium alloys as structural material: a review of research. *Eng Struct* 227:111372. <https://doi.org/10.1016/j.engstruct.2020.111372>
- Georgantzia E, Bin Ali S, Gkantou M, Kamaris GS, Kansara KD, Atherton W (2021) Flexural buckling performance of concrete-filled aluminium alloy tubular columns. *Eng Struct* 242:112546. <https://doi.org/10.1016/j.engstruct.2021.112546>
- Georgantzia E, Gkantou M, Kamaris GS (2021c) Numerical modelling and design of aluminium alloy angles under uniform compression. *CivilEng* 2(3):632–651. <https://doi.org/10.3390/civileng2030035>
- Georgantzia E, Gkantou M, Kamaris GS, Kansara KD (2022) Design of aluminium alloy channel sections under minor axis bending. *Thin-Walled Struct* 174:109098. <https://doi.org/10.1016/j.tws.2022.109098>
- Georgantzia E, Gkantou M, Kamaris GS, Kansara KD (2022b) Ultimate response and plastic design of aluminium alloy continuous beams. *Structures* 39:175–193. <https://doi.org/10.1016/j.istruc.2022.03.015>

- Georgantzia E, Gkantou M, Kamaris GS (2023) Aluminium alloy channel columns: Testing, numerical modelling and design. *Thin-Walled Struct* 182:110242. <https://doi.org/10.1016/j.tws.2022.110242>
- Georgantzia E, Finney C, Robinson A, Kashani MM (2024) Modeling nonlinear stress–strain behaviour of 6000 series aluminum alloys under cyclic loading. *J Mater Civ Eng* 36:04024133. <https://doi.org/10.1061/JMCEE7.MTENG-17314>
- Georgantzia E (2022) Structural response and design of aluminium alloy members. Ph.D. thesis. Liverpool John Moores University. Liverpool, United Kingdom.
- Giuffrè A (1970) Il comportamento del cemento armato per sollecitazioni cicliche di forte intensità. *Giornale Del Genio Civile* 28:1–20
- Gkantou M, Georgantzia E, Kadhim A, Kamaris GS, Sadique M (2023) Geopolymer concrete-filled aluminium alloy tubular cross-sections. *Structures* 51:528–543. <https://doi.org/10.1016/j.istruc.2023.02.117>
- Guo X, Xiong Z, Luo Y, Qiu L, Liu J (2015) Experimental investigation on the semi-rigid behaviour of aluminium alloy gusset joints. *Thin-Walled Struct* 87:30–40. <https://doi.org/10.1016/j.tws.2014.11.001>
- Guo X, Xiong Z, Luo Y, Xu H, Liang S (2016) Block tearing and local buckling of aluminum alloy gusset joint plates. *KSCCE J Civ Eng* 20:820–831. <https://doi.org/10.1007/s12205-015-1614-3>
- Guo X, Zhu S, Liu X, Wang K (2018) Study on out-of-plane flexural behavior of aluminum alloy gusset joints at elevated temperatures. *Thin-Walled Struct* 123:452–466. <https://doi.org/10.1016/j.tws.2017.11.045>
- Hammad A, Moustafa MA (2021) Numerical analysis of special concentric braced frames using experimentally-validated fatigue and fracture model under short and long duration earthquakes. *Bull Earthquake Eng* 19:287–316. <https://doi.org/10.1007/s10518-020-00997-8>
- Hill HN, Clark JW, Brungraber RJ (1960) Design of welded aluminum structures. *J Struct Div* 86:101–124. <https://doi.org/10.1061/JSDAEG.0000524>
- Ikeda K, Mahin SA (1986) Cyclic response of steel braces. *J Struct Eng* 112:342–361. [https://doi.org/10.1061/\(ASCE\)0733-9445\(1986\)112:2\(342\)](https://doi.org/10.1061/(ASCE)0733-9445(1986)112:2(342))
- Kashani MM (2024) Inelastic buckling of reinforcing bars: a state-of-the-art review of existing models and opportunities for future research. *Constr Build Mater* 411:134634. <https://doi.org/10.1016/j.conbuildmat.2023.134634>
- Kashani MM, Crewe AJ, Alexander NA (2013) Nonlinear cyclic response of corrosion-damaged reinforcing bars with the effect of buckling. *Constr Build Mater* 41:388–400. <https://doi.org/10.1016/j.conbuildmat.2012.12.011>
- Kashani MM, Alagheband P, Khan R, Davis S (2015) Impact of corrosion on low-cycle fatigue degradation of reinforcing bars with the effect of inelastic buckling. *Int J Fatigue* 77:174–185. <https://doi.org/10.1016/j.ijfatigue.2015.03.013>
- Kashani MM, Salami MR, Goda K, Alexander NA (2018) Non-linear flexural behaviour of RC columns including bar buckling and fatigue degradation. *Mag Concr Res* 70:231–247. <https://doi.org/10.1680/jmacr.16.00495>
- Kashani MM, Ge X, Dietz MS, Crewe AJ, Alexander NA (2019) Significance of non-stationary characteristics of ground-motion on structural damage: shaking table study. *Bull Earthquake Eng* 17:4885–4907. <https://doi.org/10.1007/s10518-019-00668-3>
- Kim TS (2012) Block shear strength of single shear four-bolted connections with aluminum alloys—experiment and design strength comparison. *Appl Mech Mater* 217–219:386–389. <https://doi.org/10.4028/www.scientific.net/AMM.217-219.386>
- Koh SK, Stephens RI (1991) Mean stress effects on low cycle fatigue for a high strength steel. *Fatigue Fract Eng Mater Struct* 14:413–428. <https://doi.org/10.1111/j.1460-2695.1991.tb00672.x>
- Kunnath SK, Heo Y, Mohle JF (2009) Nonlinear uniaxial material model for reinforcing steel bars. *J Struct Eng* 135:335–343. [https://doi.org/10.1061/\(ASCE\)0733-9445\(2009\)135:4\(335\)](https://doi.org/10.1061/(ASCE)0733-9445(2009)135:4(335))
- Lima C, Martinelli E (2019) A low-cycle fatigue approach to predicting shear strength degradation in RC joints subjected to seismic actions. *Bull Earthquake Eng* 17:6061–6078. <https://doi.org/10.1007/s10518-019-00688-z>
- Manson SS (1965) Fatigue: a complex subject—Some simple approximations. *Natl Aeronaut Space Admin* 5:193–226. <https://doi.org/10.1007/BF02321056>
- Manson SS, Hirschberg MH (1970) The role of ductility, tensile strength and fracture toughness in fatigue. *J Franklin Inst* 290:539–548. [https://doi.org/10.1016/0016-0032\(70\)90236-X](https://doi.org/10.1016/0016-0032(70)90236-X)
- Mazzolani F (1975) Residual stress tests alu-alloy Austrian profiles. ECCS Committee, Brussels
- Mazzolani FM. (2004) Design of aluminium structures. University of Naples “Federico II”, Italy. Chairman of CEN-TC. p 250
- Mazzoni S, McKenna F, Scott M, Fenves G et al. (2006) OpenSees command language manual. <https://opensees.berkeley.edu/OpenSees/manuals/usermanual/OpenSeesCommandLanguageManualJune2006.pdf>. Accessed Jan 01 2025

- Menegotto M, Pinto P (1973) Method of analysis for cyclically loaded RC plane frames including changes in geometry and non-elastic behavior of elements under combined normal force and bending. In: IABSE Symposium on Resistance and Ultimate Deformability of Structures Acted on by Well Defined Repeated Loads. International Association for Bridge and Structural Engineering, Zurich, Switzerland., pp 15–22
- Miner MA (1945) Cumulative damage in fatigue. *J Appl Mech* 12:A159–A164. <https://doi.org/10.1115/1.4009458>
- Morrow J (1968) Fatigue design handbook. *Adv Eng Soc Automot Eng* 4:21–29
- OpenSees (2011) The open system for earthquake engineering simulation. Pacific Earthquake Engineering Research Center (PEER), University of California, Berkeley, CA, USA
- Oyeniran Adeoti G, Fan F, Wang Y, Zhai X (2015) Stability of 6082–T6 aluminium alloy columns with H-section and rectangular hollow sections. *Thin-Walled Struct* 89:1–16. <https://doi.org/10.1016/j.tws.2014.12.002>
- Piluso V, Pisapia A, Nastri E, Montuori R (2019) Ultimate resistance and rotation capacity of low yielding high hardening aluminium alloy beams under non-uniform bending. *Thin-Walled Struct* 135:123–136. <https://doi.org/10.1016/j.tws.2018.11.006>
- Pisapia A, Nastri E, Piluso V, Formisano A, Mazzolani FM (2023) Experimental campaign on structural aluminium alloys under monotonic and cyclic loading. *Eng Struct*. <https://doi.org/10.1016/j.engstruct.2023.115836>
- Ramberg W, Osgood W (1943) Description of stress-strain curves by three parameters. National Advisory Committee for Aeronautics. Washington, D.C. Accessed Jan 01 2025 <https://ntrs.nasa.gov/api/citations/19930081614/downloads/19930081614.pdf>
- Spacone E, Filippou F, Taucer F (1996a) Fibre beam-column model for non-linear analysis of R/C frames: part I. Formulation. *Earthq Eng Struct Dyn* 25:711–725. [https://doi.org/10.1002/\(SICI\)1096-9845\(199607\)25:7%3c711::AID-EQE576%3e3.0.CO;2-9](https://doi.org/10.1002/(SICI)1096-9845(199607)25:7%3c711::AID-EQE576%3e3.0.CO;2-9)
- Spacone E, Filippou F, Taucer F (1996b) Fibre beam-column model for non-linear analysis of R/C frames: part II. Applications. *Earthq Eng Struct Dyn* 25:727–742. [https://doi.org/10.1002/\(SICI\)1096-9845\(199607\)25:7%3c727::AID-EQE577%3e3.0.CO;2-O](https://doi.org/10.1002/(SICI)1096-9845(199607)25:7%3c727::AID-EQE577%3e3.0.CO;2-O)
- Stojadinovic B (2003) Stability and low-cycle fatigue limits of moment connection rotation capacity. *Eng Struct* 25:691–700. [https://doi.org/10.1016/S0141-0296\(02\)00178-5](https://doi.org/10.1016/S0141-0296(02)00178-5)
- The MathWorks Inc. (2022) Optimization Toolbox version: 9.4 (R2022b). <https://www.mathworks.com>. Accessed 10 May 2023
- Timoshenko S, Gere J (1961) *Theory of Elastic Stability*, 2nd edn. McGraw-Hill Book Co., Inc., New York
- Tremblay R, Archambault M-H, Filiatrault A (2003) Seismic response of concentrically braced steel frames made with rectangular hollow bracing members. *J Struct Eng* 129:1626–1636. [https://doi.org/10.1061/\(ASCE\)0733-9445\(2003\)129:12\(1626](https://doi.org/10.1061/(ASCE)0733-9445(2003)129:12(1626)
- Uriz P (2005) Towards earthquake resistant design of concentrically braced steel structures. Ph.D. thesis. University of California, Berkeley, CA, USA
- Xiang P, Jia L-J, Shi M, Wu M (2017) Ultra-low cycle fatigue life of aluminum alloy and its prediction using monotonic tension test results. *Eng Fract Mech* 186:449–465. <https://doi.org/10.1016/j.engfracmech.2017.11.006>
- Yahya MM, Mallik N, Chakrabarty I (2015) Low cycle fatigue (LCF) behavior of AA6063 aluminium alloy at room temperature. *Int J Emerg Technol Adv Eng* 5:100–108
- Zhu JH, Young B (2006) Aluminum alloy tubular columns-Part I: Finite element modeling and test verification. *Thin-Walled Struct* 44:961–968. <https://doi.org/10.1016/j.tws.2006.08.011>

**Publisher's Note** Springer Nature remains neutral with regard to jurisdictional claims in published maps and institutional affiliations.